Split Shock Waves from Molecular Dynamics

D. H. Robertson, D. W. Brenner, and C. T. White
Naval Research Laboratory, Washington, D.C. 20375-5000
(Received 3 October 1991)

We show that the generation and evolution of split shock waves resulting from a dissociative polymorphic phase transition can be modeled using molecular-dynamics (MD) simulations. A model 2D semi-infinite molecular solid, driven with a piston, exhibits both single and split shock waves depending on the piston velocity. The results obtained from these MD simulations are in excellent agreement with continuum theory. These results—explicitly treating fewer than 5000 atoms—demonstrate that MD simulations provide a promising tool for studying the interplay between shock waves and polymorphic phase transitions.

PACS numbers: 62.50.+p, 47.40.Nm, 82.40.Fp

As early as 1956, Bancroft, Peterson, and Minshall reported experimental data which demonstrated that polymorphic phase transitions in iron can be produced by dynamic shock-wave loading [1]. Following their discovery, shock-wave techniques combined with static measurements were used to determine the high-pressure phase diagram of iron. Since then many other shock-induced phase transitions have been profitably studied [2]. A notable example is the shock compression of graphite or soot to produce diamond [3]. An important property of these shock-induced transitions is the accompanying shock-wave splitting that may occur. Shock-wave splitting led to the original discovery of these transitions [4] and continues to be exploited in their study [5].

Theories of shock-induced transitions have so far concentrated on relating static to dynamic measurements, with little if any attention given to simulating these dynamically induced transitions using molecular dynamics (MD). This state of affairs is surprising, because shock waves occur on such a short time and length scale—traversing typically 50 Å or more in a picosecond—they are often ideal for MD studies. Indeed, MD methods have not only been successfully used to model shock waves in systems without polymorphic transitions [6], but also to model pressure-induced polymorphic transitions under static but not dynamic inertial confinement [7]. Therefore, this method would seem a promising tool for studying the interplay between shock waves and the polymorphic transitions they can induce, provided these transitions occur on a time scale accessible to the simulations.

In this Letter we report results from MD simulations for a 2D diatomic molecular solid which exhibits a shock-induced phase transition and a concomitant split shock wave. Remarkably—even when the transition, accompanied by a large volume change, is present—we find that the results of these nanoscale simulations are in excellent agreement with the Rankine-Hugoniot relations from continuum theory that relate the steady-state macroscopic flow variables across the shock front.

The 2D model used in these studies is based on many-body Tersoff-type potentials [8] which represent the total potential energy of a collection of N atoms as

$$V=\sum_{i}^{N}\sum_{j>i}^{N} f_c(r_{ij})[V_R(r_{ij})-\bar{B}_{ij}V_A(r_{ij})]+V_{\mathrm{vdW}}(r_{ij}), \quad (1)$$

where the parameters and functions used in this expression are given in Table I. The molecular bonding portion of the potential consists of a repulsive, V_R, and an attractive, V_A, term, both modeled using generalized Morse potentials. The bond order function, $\bar{B}_{ij}\equiv(B_{ij}+B_{ji})/2$, introduces many-body effects into the potential by modifying V_A according to the local bonding environment. Here $\bar{B}_{ij}$ is chosen to favor a valence of one, insuring that without the van der Waals bonding term V_{vdW} the ground state at zero temperature and pressure is a collection of $N/2$ independent diatomic molecules. For the parameters given in Table I, each of these diatomic molecules has a binding energy of 5 eV and a vibrational frequency of 1682 cm^{-1} at an equilibrium bond distance of 1.0 Å, all similar to molecular oxygen. Inclusion of V_{vdW} causes this system to condense into a diatomic molecular solid which in two dimensions has a crystalline binding energy of 0.04 eV per molecule, a distance of closest approach between atoms in nearest-neighboring molecules of 3.3 Å, and a solid-state speed of sound of 1.9 km/s, all well within physical norms.

With increasing hydrostatic pressure this diatomic molecular solid (DMS) becomes unstable with respect to a close-packed solid (CPS) at a 2D pressure of about 1 $\mathrm{eV/Å}^2$ which corresponds to an effective 3D pressure [9] near 40 GPa. The density of this CPS for pressures immediately above the transition relative to the density of the initial DMS at near zero temperature and pressure, $\rho_{\mathrm{CPS}}/\rho_{\mathrm{DMS}}$, is 2.5. Accompanying this transition the nearest-neighbor interatomic distance d_{NN} increases by about 20% due primarily to a decrease in $\bar{B}_{ij}$ with an increasing number of nearest neighbors. All these properties of the model make this DMS to CPS transition similar to the dissociative transition reported in diatomic molecular solids of iodine [10] and bromine [11]. This transition occurs at 21 GPa in I_2 and 81 GPa in Br_2, leading to an increase in the overall relative density, $\rho_{\mathrm{CPS}}/\rho_{\mathrm{DMS}}$, of 1.7 for I_2 and 2.3 for Br_2, and an increase in

TABLE I. The components and parameters used in Eq. (1). In the simulations each atom was assumed to have the mass of N.

$V_R(r)=[D_e/(S-1)]\exp[-\alpha\sqrt{2S}(r-r_e)]$	$D_e=5.0$ eV
	$S=1.8$
	$\alpha=2.7$ Å^{-1}
$V_A(r)=[SD_e/(S-1)]\exp[\alpha\sqrt{2/S}(r-r_e)]$	$r_e=1$ Å
	$G=5.0$
$B_{ij}=\left(1+G\sum_{k\neq i,j}f_c(r_{ij})\exp[m(r_{ij}-r_{ik})]\right)^{-n}$	$m=2.25$ Å^{-1}
	$n=0.5$
$f_c(r)=\begin{cases}1, & r<2\\ \frac{1}{2}\{1+\cos[\pi(r-2)]\}, & 2\le r<3\\ 0, & 3\le r\end{cases}$	$\epsilon=5.0\times10^{-3}$ eV
	$\sigma=2.988$ Å
	$P_0=0.4727$ eV Å^{-1}
	$P_1=-0.6996$ eV Å^{-1}
$V_{\mathrm{vdW}}(r)=\begin{cases}0, & r<1.75\\ P_0+r[P_1+r(P_2+rP_3)], & 1.75\le r<2.91\\ 4\epsilon[(\sigma/r)^{12}-(\sigma/r)^6], & 2.91\le r<7.32\\ 0, & 7.32\le r\end{cases}$	$P_2=0.3364$ eV Å^{-1}
	$P_3=-0.0520$ eV Å^{-1}

d_{NN} of around 15% for both materials. The model, however, predicts that 50% of the overall density change occurs at the transition, while in I_2 and Br_2 the change is 6%. Much of this difference arises because the ratio of the van der Waals to diatomic bond length, R, in the model is considerably larger than the corresponding ratio in either I_2 or Br_2. We have not attempted to alter this feature of the model because a larger R is a realistic feature of other molecular solids. This larger change in density at the transition should also increase the relaxation time necessary to achieve local equilibrium and hence *will provide* an even more severe test of the ability of MD to model such shock-induced dissociative transitions.

Shock waves in the MD simulations are produced by driving the free edge of the molecular solid initially at rest at near zero temperature and pressure with a rigid layer of atoms moving at a constant velocity. The dynamics of the remaining atoms are then propagated by integrating Hamilton's equations of motion using a Nordsieck predictor-corrector method with a variable time step [12]. Various shock velocities are obtained by starting with different initial piston velocities leading to different final shocked states. During the simulations, cyclic boundary conditions are enforced perpendicular to the direction of shock propagation. The results reported below were all obtained by explicitly treating the motion of fewer than 5000 atoms for less than 20 ps.

Snapshots of the simulations for piston velocities of 2.0, 5.0, and 8.0 km/s (from top to bottom) are given in Fig. 1. The location of the resulting shock-wave fronts are clearly visible as sharp changes in density between adjacent regions. The shock front velocities calculated from the MD simulations were found to approach a constant time-averaged velocity in anywhere between 2.4 and 12 ps, with the longer times corresponding to simulations which had a piston velocity just above that needed to induce the split shock wave. These averaged front velocities are plotted as a function of the piston velocities in Fig. 2. The solid lines in Fig. 2 are polynomial fits to the plotted points. A cubic polynomial was used to fit the data for less than or equal to 3.0 km/s, an average was used for the almost horizontal data, and a linear fit was used for the remaining data. Continuum theory predicts that in the limit of infinitesimal piston velocities the shock velocity should approach the speed of sound in the unshocked material [13]. The shock velocity in this limit extrapolated from the cubic fit to the MD data is 1.8 km/s, which is in good agreement with the longitudinal

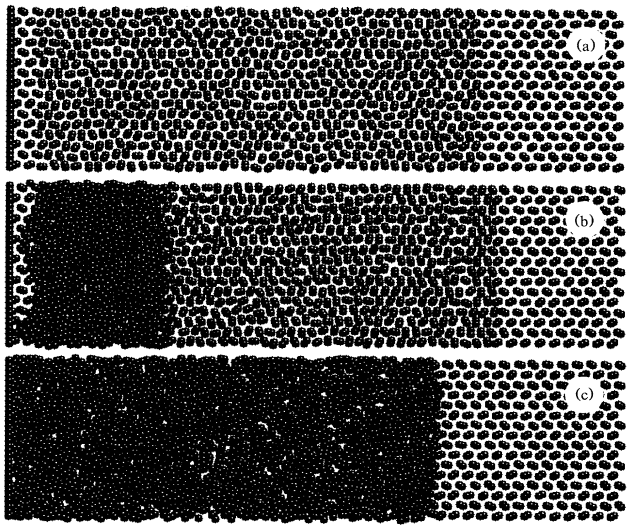

FIG. 1. Snapshots of the simulations for piston velocities of (a) 2.0, (b) 5.0, and (c) 8.0 km/s. The shock waves are propagating from left to right.

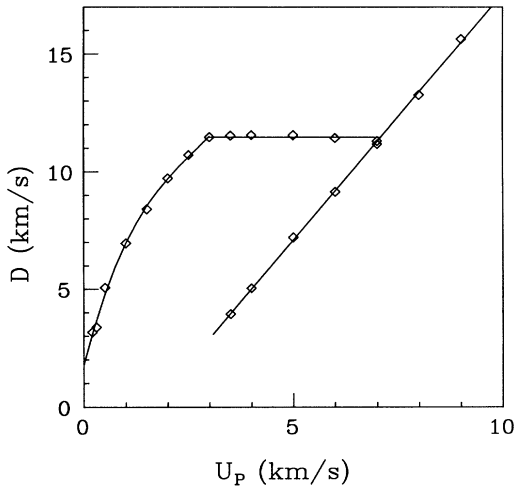

FIG. 2. Velocities of the shock waves, D, calculated from the MD simulations as a function of the piston velocity U_P.

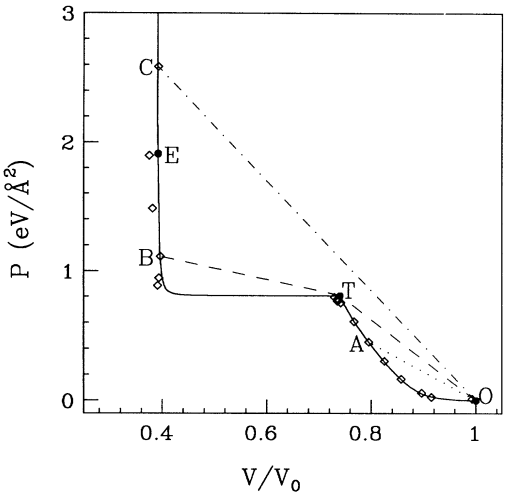

FIG. 3. The Hugoniot for the model system. The solid circles O, T, and E correspond to the initial state, the onset of the transition, and the point such that line OE just touches the Hugoniot at T, respectively. The diamonds A, B, and C are the final states for the piston velocities used to generate Figs. 1(a), 1(b), and 1(c), respectively.

speed of sound in the unshocked material, 1.9 km/s, calculated using a different method [14].

As can be seen from Fig. 2, at piston velocities below 3.0 km/s only one shock wave is present [Fig. 1(a)]. When the piston velocity exceeds about 3.0 km/s a polymorphic transition accompanied by a split shock wave is observed [Fig. 1(b)]. In the range of piston velocities where a split shock wave is present, the velocity of the first shock wave remains near constant at 11.5 km/s while the velocity of the second front continues to increase with increasing piston velocities. At a piston velocity of 7.1 km/s or greater the velocity of the second shock wave exceeds that of the first, and only the second wave remains [Fig. 1(c)]. Across this remaining second front the molecular solid at initial conditions transforms directly to the close-packed solid. All of these results are in agreement with continuum theory [13] as we now show.

The continuum theory of planar shock waves at steady flow conditions leads to the Rankine-Hugoniot relations [15]:

$$D = V_0[(P-P_0)/(V_0-V)]^{1/2}, \tag{2}$$

$$u_p = [(V_0-V)(P-P_0)]^{1/2}, \tag{3}$$

$$\epsilon(P,V) - \epsilon(P_0,V_0) = Pu_pV_0/D - u_p^2/2, \tag{4}$$

in the reference frame where the material preceding the front is stationary. Assuming the equation of state giving $\epsilon(P,V)$ is known, these relations determine the locus of all final states defined by the specific volume V, pressure P, and flow velocity u_p that can be reached by shock compression of the initial state characterized by V_0, P_0, and the shock velocity D. Equations (2) and (3) can then be used to eliminate u_p and D from Eq. (4) leading to a curve in P-V space, $P = H(V;V_0,P_0)$, known as the Hugoniot. The Hugoniot for the model is given in Fig. 3.

The diamonds in Fig. 3 are the values of V and P computed directly from the simulations [16] at locations approximately 20 Å behind the shock front after the velocities of these fronts have stabilized. The solid curves in Fig. 3 are computed by using Eqs. (2) and (3) to convert the D vs U_P solid curves in Fig. 2 to the P vs V Hugoniot relationship. The close agreement between these results confirms that near steady flow conditions have been reached over the entire range of piston velocities studied.

The level of agreement depicted in Fig. 3 also shows that the occurrence of split shock waves in the simulations can be understood using the first two Rankine-Hugoniot relations and the computed Hugoniot [1,2,13]. First, consider a final state such as A shown in Fig. 3 which corresponds to the piston velocity used to generate Fig. 1(a). This final state lies between the initial state $O(P_0,V_0)$ and the point $T(P_T,V_T)$ on the Hugoniot where the transition begins. For such a final state a straight line (Rayleigh line) such as OA shown in Fig. 3 can be drawn from the initial to final state without otherwise intersecting the Hugoniot. Therefore, there will be only a single shock wave present in the material. This conclusion follows from Eq. (2) which implies that the slope of the Rayleigh line OA is proportional to the shock velocity and the observation that P is a nondecreasing function of the shock compression. Because A lies between O and T this single shock wave compresses and heats the undisturbed material and starts it flowing but does not induce a phase transition as depicted in Fig. 1(a). Also, because there is only a single shock wave present, u_p coincides with the piston velocity U_P so that Eq. (3) implies that such an ordinary shock wave will al-

ways result provided $U_P < U_P^T \equiv [(V_0 - V_T)(P_T - P_0)]^{1/2} \approx 3.0$ km/s.

Next, consider a final state such as C shown in Fig. 3 which corresponds to Fig. 1(c). This final state lies beyond this point E shown in Fig. 3; E is defined as the intersection of the Hugoniot with the Rayleigh line OE that just touches the Hugoniot at the point T. Again there will be only a single shock wave present in the material because the Rayleigh line OC, shown in Fig. 3, can be drawn without otherwise intersecting the Hugoniot. Here, however, C lies beyond T so that the transition takes place across this single front as depicted in Fig. 1(c). Also, Eq. (3) now implies that such a final state will always result provided $U_P > U_P^E \equiv [(V_0 - V_E)(P_E - P_0)]^{1/2} \approx 7.1$ km/s.

Last, consider a final state such as B shown in Fig. 3 which corresponds to Fig. 1(b). This final state lies between T and E and hence is generated by a piston velocity between U_P^T and U_P^E. For such a final state a single Rayleigh line cannot be drawn from O to B without otherwise intersecting the Hugoniot. Therefore, the shock wave splits into two independent waves moving at different speeds. The first shock wave starts the material moving, compressing and heating it to the point of transition, T, while the transition takes place across the second front bringing the material to the final state B. Equations (2) and (3) imply that the first shock propagates with respect to the material immediately behind it at a velocity given by $D - u_p = V_T[(P_T - P_0)/(V_0 - V_T)]^{1/2}$, while Eq. (2) implies that the second wave propagates into this compressed, heated, and moving material with a velocity given by $V_T[(P_B - P_T)/(V_T - V_B)]^{1/2}$. Because B lies between T and E the slope of the line OT must exceed the slope of the line TB and hence these two waves separate as depicted in Fig. 1(b). This analysis also demonstrates why when split shock waves are present the velocity of the leading wave will always be pinned at $V_0[(P_T - P_0)/(V_0 - V_T)]^{1/2} \approx 11.5$ km/s.

These results establish for the first time that MD simulations can be successfully used to model such complex dynamic phenomena as split shock waves caused by a polymorphic phase transition. Given the relatively small size (< 5000 atoms) and short times (< 20 ps) needed to achieve near steady flow conditions in our 2D model, a wide range of related phenomena should soon become accessible to MD simulations. New numerical algorithms that can follow the dynamics of up to 10^6 atoms on parallel computers [17] should soon make possible 3D simulations using realistic many-body potentials that, for example, could lead to a better understanding of the significant differences between static [18] and shock [19] results for solid N_2.

This work was supported by ONR and a grant in computer time from the NRL Research Advisory Committee. D.H.R. acknowledges a NRC-NRL Postdoctoral Research Associateship.

[1] D. Bancroft, E. L. Peterson, and S. Minshall, J. Appl. Phys. **27**, 291 (1956).
[2] G. E. Duvall and R. A. Graham, Rev. Mod. Phys. **49**, 523 (1977).
[3] P. S. DeCarli and J. C. Jamieson, Science **133**, 1821 (1961).
[4] S. Minshall, Phys. Rev. **98**, 271 (1955).
[5] D. J. Erskine and W. J. Nellis, Nature (London) **349**, 317 (1991).
[6] B. L. Holian, W. G. Hoover, B. Moran, and G. K. Straub, Phys. Rev. A **22**, 2798 (1980).
[7] J. R. Ray and A. Rahman, Physica (Amsterdam) **150B**, 250 (1988); K. Y. Lee and J. R. Ray, Phys. Rev. B **39**, 565 (1989).
[8] J. Tersoff, Phys. Rev. Lett. **56**, 632 (1986); Phys. Rev. B **37**, 6991 (1988).
[9] This effective 3D pressure is calculated by assuming a vertical distance equal to the distance of closest approach between atoms in nearest-neighboring molecules in the plane.
[10] K. Takemura, S. Minomura, O. Shimomura, Y. Fujii, and J. D. Axe, Phys. Rev. B **26**, 998 (1982).
[11] Y. Fujii, K. Hase, Y. Ohishi, H. Fujihisa, N. Hamaya, K. Takemura, O. Shimomura, T. Kikegawa, Y. Amemiya, and T. Matsushita, Phys. Rev. Lett. **63**, 536 (1989).
[12] C. W. Gear, *Numerical Initial Value Problems in Ordinary Differential Equations* (Prentice-Hall, Englewood Cliffs, 1971), p. 148.
[13] Ya. B. Zel'dovich and Yu. P. Raizer, *Physics of Shockwaves and High Temperature Hydrodynamic Phenomena* (Academic, New York, 1967), Vol. 1, p. 56; *ibid.*, Vol. 2, Sec. 19.
[14] D. A. McQuarrie, *Statistical Mechanics* (Harper and Row, New York, 1976), pp. 208, 544, and 572.
[15] See, e.g., M. Ross, in *Encyclopedia of Physics,* edited by R. G. Lerner and G. L. Trigg (Addison-Wesley, London, 1981), p. 924.
[16] R. J. Hardy, J. Chem. Phys. **76**, 622 (1982).
[17] B. L. Holian, A. J. De Groot, W. G. Hoover, and C. G. Hoover, Phy. Rev. A **41**, 4552 (1990).
[18] R. Reichlin, D. Schiferl, S. Martin, C. Vanderborgh, and R. L. Mills, Phys. Rev. Lett. **55**, 1464 (1985).
[19] H. B. Radousky, W. J. Nellis, M. Ross, D. C. Hamilton, and A. C. Mitchell, Phys. Rev. Lett. **57**, 2419 (1986).